

Too Big to Fail in the Local Group

Shea Garrison-Kimmel^{1*}, Michael Boylan-Kolchin², James S. Bullock¹,

Evan N. Kirby^{1,3}

¹*Center for Cosmology, Department of Physics and Astronomy, University of California, Irvine, CA 92697, USA*

²*Department of Astronomy and Joint Space-Science Institute, University of Maryland, College Park, MD 20742-2421, USA*

³*Center for Galaxy Evolution Fellow*

23 April 2014

ABSTRACT

We compare the dynamical masses of dwarf galaxies in the Local Group (LG) to the predicted masses of halos in the ELVIS suite of Λ CDM simulations, a sample of 48 Galaxy-size hosts, 24 of which are in paired configuration similar to the LG. We enumerate unaccounted-for dense halos ($V_{\max} \gtrsim 25 \text{ km s}^{-1}$) in these volumes that at some point in their histories were massive enough to have formed stars in the presence of an ionizing background ($V_{\text{peak}} > 30 \text{ km s}^{-1}$). Within 300 kpc of the Milky Way, the number of unaccounted-for massive halos ranges from 2 – 25 over our full sample. Moreover, this “too big to fail” count grows as we extend our comparison to the outer regions of the Local Group: within 1.2 Mpc of either giant we find that there are 12-40 unaccounted-for massive halos. This count excludes volumes within 300 kpc of both the MW and M31, and thus should be largely unaffected by any baryonically-induced environmental processes. According to abundance matching – specifically abundance matching that reproduces the Local Group stellar mass function – all of these missing massive systems should have been quite bright, with $M_{\star} > 10^6 M_{\odot}$. Finally, we use the predicted density structure of outer LG dark matter halos together with observed dwarf galaxy masses to derive an $M_{\star} - V_{\max}$ relation for LG galaxies that are outside the virial regions of either giant. We find that there is no obvious trend in the relation over three orders of magnitude in stellar mass (a “common mass” relation), from $M_{\star} \sim 10^8 - 10^5 M_{\odot}$, in drastic conflict with the tight relation expected for halos that are unaffected by reionization. Solutions to the too big to fail problem that rely on ram pressure stripping, tidal effects, or statistical flukes appear less likely in the face of these results.

Key words: dark matter – cosmology: theory – galaxies: haloes – Local Group

1 INTRODUCTION

Numerical simulations of structure formation have emerged as a standard technique for making and testing predictions of the Λ CDM model of hierarchical galaxy formation (Davis et al. 1985; Frenk et al. 1988; Warren et al. 1992; Gelb & Bertschinger 1994; Cen et al. 1994; Hernquist et al. 1996; Gross et al. 1998; Jenkins et al. 2001; Wambsganss et al. 2004; Springel et al. 2005; Boylan-Kolchin et al. 2009; Klypin et al. 2011). These studies have been remarkably successful at reproducing the large-scale properties of the Universe, but disagreements have periodically emerged on smaller scales.

The smallest dwarf galaxies (stellar mass $M_{\star} \lesssim 10^8 M_{\odot}$) can be detected and studied best locally, and thus many of these small-scale problems have been identified by compar-

ing observations of Milky Way (MW) satellites with subhalos of simulated MW-size hosts. For example, the “missing satellites problem” (Kauffmann et al. 1993; Klypin et al. 1999; Moore et al. 1999; Bullock 2010), points out that although dark matter (DM)-only simulations predicted a wealth of collapsed substructure around the MW, only ~ 10 bright satellite galaxies are known. Though the known count of MW satellites has more than doubled in the past ten years, all of these new satellites have been of fairly low mass (e.g. Willman et al. 2005; Belokurov et al. 2006, 2007). Moreover, even allowing for these new detections in the overall count, one must still assume that only a small percentage of subhalos are populated by luminous galaxies in order to explain the discrepancy. It is typical to assume that the brightest “classical” dwarf spheroidal (dSph) galaxies are hosted by the largest subhalos typical of MW-size hosts ($V_{\max} \sim 30 \text{ km s}^{-1}$).

* sgarriso@uci.edu

The idea that the most luminous galaxies reside in the most massive halos is reinforced by the success of the abundance matching (AM) technique, which accurately reproduces clustering statistics and luminosity functions for $M_* > 10^8 M_\odot$ galaxies (Kravtsov et al. 2004; Vale & Ostriker 2004; Conroy et al. 2006; Behroozi et al. 2013c; Moster et al. 2013). Specifically, AM provides an $M_* - M_{\text{halo}}$ relation by matching DM halo mass functions from cosmological simulations with stellar mass functions from large-volume surveys, implicitly assuming that the most luminous galaxies reside in the largest dark matter halos. If one extrapolates AM to the dwarf scale, the resultant satellite stellar mass functions agree well with those of the MW and M31 satellites for $M_* \gtrsim 10^5 M_\odot$ (Koposov et al. 2009; Busha et al. 2010; Kravtsov 2010; Lunnan et al. 2012; Boylan-Kolchin et al. 2012; Brook et al. 2013; Garrison-Kimmel et al. 2014). Below $M_* \sim 10^5 M_\odot$, the abundance of galaxies may become more strongly suppressed than expected in power-law AM extrapolations because the smallest subhalos ($V_{\text{peak}} < 30 \text{ km s}^{-1}$) may not have formed stars because of reionization (Bullock et al. 2000; Somerville 2002; Sawala et al. 2014). As discussed in Garrison-Kimmel et al. (2014), surveys like LSST will test this possibility.

With the advent of the zoom-in technique (Katz & White 1993; Oñorbe et al. 2014), which focuses the majority of the computational power of a cosmological simulation on a small high-resolution region, simulations can now test whether these largest subhalos are indeed compatible with the luminous MW dSphs, as AM predicts.

Boylan-Kolchin et al. (2011, 2012) used the zoom-in simulations of the Aquarius Suite (Springel et al. 2008), which includes six ultra-high resolution MW-size hosts, to compare the internal kinematics of the massive subhalos of MW hosts to the brightest MW satellites (those with $M_* > 10^5 M_\odot$). They discovered that measurements of the stellar velocity dispersions, σ_* , indicate systematically lower central mass estimates than simulations predict for large subhalos – that is, the MW dSphs are systematically less dense than the subhalos expected to host them, a problem that has been dubbed “Too Big to Fail” (TBTf). While possibly related to the missing satellites problem, in that the largest subhalos may not have been found, TBTf is a distinct problem related to the internal structure of subhalos, rather than strictly their abundances. However, it could be alleviated by the discovery of several new high-density dwarf satellites.

TBTf may also be tied to the shapes of the inner density profiles of dwarf halos. Collisionless simulations predict cuspy central regions, whereas measurements by Walker & Peñarrubia (2011), Jardel & Gebhardt (2012), Agnello & Evans (2012), and Amorisco et al. (2013a) indicate cored matter distributions in the larger dSphs (Fornax and Sculptor), similar to the cusp-core problem in slightly more massive low surface brightness galaxies (Flores & Primack 1994; Moore 1994; Kuzio de Naray et al. 2008; Trachternach et al. 2008; de Blok 2010; Kuzio de Naray & Kaufmann 2011). The slope of the central density profiles are still under debate, however – Breddels & Helmi (2013) found that it is unlikely that Fornax, Sculptor, Carina, and Sextans are hosted by cored dark matter halos. The TBTf problem is independent of the inner slope, however, as it is phrased in terms of the integrated mass within the half-light radii of dwarfs,

quantities that are much more robustly determined observationally than density profile slopes.

There have been a number of suggestions proposed for resolving TBTf. Some authors have pointed out that self-interactions in the dark matter naturally lead to 0.5 – 1 kpc cores in dwarf subhalos (Vogelsberger et al. 2012; Rocha et al. 2013; Elbert et al. in prep), though there are indications that the self-interaction cross section must be velocity dependent to satisfy other constraints (Zavala et al. 2013). Others have investigated whether TBTf may be a result of the underlying cosmology of the Aquarius simulations, where TBTf was first identified, such as the adopted values of σ_8 and n_s (Polisensky & Ricotti 2014) or the assumed coldness of the dark matter (Anderhalden et al. 2013; Lovell et al. 2013, and references therein). Others have argued that TBTf is a result of the mass of the targeted halos, pointing to simulations that indicate that smaller hosts, $M_v \sim 8 \times 10^{11} M_\odot$, do not typically contain these large, dense subhalos (Di Cintio et al. 2011; Wang et al. 2012; Vera-Ciro et al. 2013). It may also be that a fraction of the MW-size halos in the Universe do not host these dense subhalos (Purcell & Zentner 2012), though the statistical study of Rodríguez-Puebla et al. (2013) found that the TBTf problem is typical of MW-size hosts.

Many authors have also noted that TBTf was first identified in collisionless simulations, which do not account for baryonic forces, and that it is therefore possible that these missing physics, such as supernova feedback, ram pressure stripping, and tidal interactions, may account for the discrepancy (e.g. Pontzen & Governato 2012; Zolotov et al. 2012; Arraki et al. 2013; Brooks & Zolotov 2012; Del Popolo 2012; Brooks et al. 2013; Gritschneider & Lin 2013; Amorisco et al. 2013b; Del Popolo et al. 2014). Although energetic arguments indicate that the former is unlikely in most cases (Peñarrubia et al. 2012; Garrison-Kimmel et al. 2013), there is ample evidence that dwarfs are strongly affected by their environment – for example, there are only two galaxies within 300 kpc of the MW with detected gas (the Magellanic Clouds); conversely, there are only two known gas-free field dwarfs within ~ 1 Mpc of the MW (Cetus and Tucana; Grcevich & Putman 2009; McConnachie 2012).

Thus far, work on TBTf has focused largely on the subhalos and dSph satellites of the MW, while Tollerud et al. (2014) have shown the same issue is seen around M31. To eliminate the uncertain effects introduced by environment, however, one should study galaxies beyond the virial radii of the MW and M31, where ram pressure and tidal stripping are minimal. Isolated dwarf galaxies in the Local Field (a term we will use to refer to the region within 1.2 Mpc of either the MW or M31, but more than 300 kpc from both) do not appear to be denser than the MW dSphs (Kirby et al. 2014), but predictions for halo properties in the Local Field have thus far been sparse.

In this paper, we examine both satellite and field dwarf halos around the hosts of the Exploring the Local Volume in Simulations (ELVIS) Suite (Garrison-Kimmel et al. 2014, hereafter GK14), a set of zoom-in simulations focused on LG-like environments that resolve ~ 3 Mpc regions without contamination from low resolution particles, for the TBTf problem. Specifically, we count the number of “massive failures” – large halos ($V_{\text{peak}} > 30 \text{ km s}^{-1}$) that do not have luminous counterparts – both within 300 kpc of the 48 MW-

size hosts and in the fields surrounding the LG analogs. Because the ELVIS Suite adopts cosmological parameters from the WMAP-7 results ($\sigma_8 = 0.801$, $\Omega_m = 0.266$, $\Omega_\Lambda = 0.734$, $n_s = 0.963$, and $h = 0.71$; Larson et al. 2011), which includes a significantly lower value of σ_8 than the WMAP-1 parameter set adopted for the Aquarius simulations, we will also test whether an updated cosmology alleviates the problem. As we show below, however, we predict that there are many such unaccounted-for dense halos throughout the Local Volume. If these halos preferentially host low-luminosity or low-surface brightness galaxies, then future surveys may detect them.

This paper is organized as follows. In §2, we briefly describe the simulations and analysis pipeline used in this work. In §3, we present empirical scaling relations between the structural parameters of subhalos and field halos and explicitly compare the properties of small halos near isolated hosts with those in paired environments. §4 presents the counts of massive failures around each host both within 300 kpc of each host (§4.1) and in the field surrounding the Local Group analogs (§4.2.1), as well as a discussion of incompleteness (§4.2.2). We conclude with an analysis of the relationship between M_\star and V_{\max} for the known dwarfs in the Local Field in §4.3. Our results are summarized in §5.

2 SIMULATIONS: THE ELVIS SUITE

The simulations used in this work, the ELVIS Suite, are described in detail in GK14. The large scale properties of the LG analogs and the individual properties of the paired and isolated halos (along with their identifying names) are given in that work. Here we briefly summarize the simulations and the analysis pipeline used in this paper.

The suite is comprised of 36 collisionless simulations, half of which are focused on a pair of dark matter halos whose masses, relative kinematics, and environments are similar to the dark matter halos that host the MW and Andromeda (M31) galaxies. The remaining twenty-four simulations are focused on isolated halos that are mass-matched to those in the pairs. Because the mass estimates for the MW and M31 agree within errors (van der Marel et al. 2012; Boylan-Kolchin et al. 2013), both hosts in each paired simulation may separately be considered as an MW analog; the ELVIS Suite therefore contains a total of 48 MW-size systems. The distribution of virial masses¹ M_v of the ELVIS hosts nearly evenly samples the mass range between $10^{12}M_\odot$ and $2.85 \times 10^{12}M_\odot$. All halos in the suite were simulated with a $z = 0$ Plummer equivalent force softening of 141 pc in the high resolution region, which contains particles with a mass $m_p = 1.89 \times 10^5 M_\odot$. Additionally, three of the isolated hosts were re-simulated with a factor of 2^3 more particles ($m_p = 2.4 \times 10^4 M_\odot$) in the high-resolution region and a corresponding $z = 0$ softening length of 70 pc. We use these runs to demonstrate the convergence of subhalo structural parameters in Appendix A.

Bound substructures are identified with **Rockstar**, a six dimensional friend-of-friends halo finder (Behroozi et al.

2013a). For this analysis, the relevant properties are V_{\max} , the maximum of the circular velocity profile, and R_{\max} , the radius at which the circular velocity peaks. We additionally select halos that are expected to have formed stars based upon V_{peak} , which is defined as V_{\max} of the main branch of the halo’s merger tree, built with **Consistent Trees** (Behroozi et al. 2013b), at the timestep when the halo reaches its maximal mass (see GK14 for more details).

Each run in the ELVIS Suite was initialized with a large high-resolution region to specifically enable study beyond the virial radius of the giant halos without contamination due to low resolution (high mass) particles. Specifically, only four (Thelma & Louise, Sonny & Cher, Hall & Oates, and Siegfried & Roy) of the twelve LG realizations contain such contaminating particles within 1.2 Mpc of either halo center. In those cases, moreover, the contamination is minimal: within 1.2 Mpc of either halo center, the contamination by mass is only 0.06%, 0.01%, 0.007%, and 0.0008%, respectively. In addition, the nearest low resolution particles in these four systems are quite distant: 0.8 Mpc, 0.97 Mpc, 1.01 Mpc, and 1.09 Mpc. Catalogs of halos in the fields around the ELVIS hosts are therefore complete and nearly entirely free of contamination at much larger distances than previous high-resolution simulations (the well known CLUES project, Gottloeber et al. 2010, and recent work by Sawala et al. 2014, are notable exceptions).

The goal of this work is to compare predicted halo densities to those of LG dwarfs at scales comparable to their observed half-light radii ($\sim 200 - 1000$ pc). Because our fiducial set of simulations lacks the resolution required make direct predictions at scales below ~ 1000 pc, we instead use the well-converged structural parameters (V_{\max} and R_{\max}) together with several reasonable choices for analytic profiles in order to extrapolate to the scales of observed dwarfs.

R_{\max} and V_{\max} together uniquely define a Navarro-Frenk-White (NFW; Navarro et al. 1996) profile:

$$\rho(r) = \rho_0 \left(\frac{2.1626 r}{R_{\max}} \right)^{-1} \left(1 + \frac{2.1626 r}{R_{\max}} \right)^{-2}, \quad (1)$$

where ρ_0 is defined such that the mass within R_v is equal to M_v . For a given shape parameter α , one may also calculate a unique Einasto profile (Einasto 1965) based upon R_{\max} and V_{\max} , though the scalings between the characteristic radius r_{-2} and R_{\max} and between ρ_{-2} , the density at r_{-2} , and V_{\max} depend upon the shape parameter:

$$\rho(r) = \rho_{-2} \exp \left(-\frac{2}{\alpha} \left[\left(\frac{A(\alpha) r}{R_{\max}} \right)^\alpha - 1 \right] \right), \quad (2)$$

where $r_{-2} = R_{\max}/A(\alpha)$. Appendix B defines $A(\alpha)$ and explicitly compares the NFW and Einasto profiles.

As mentioned above, in addition to the forty-eight halos simulated at the fiducial resolution, the ELVIS Suite also contains high-resolution re-simulations of three of the isolated hosts. We use these halos to ensure the convergence of V_{\max} and R_{\max} (see Appendix A) and find that a power law fit to the $R_{\max} - V_{\max}$ relationship,

$$\left(\frac{R_{\max}}{1 \text{ kpc}} \right) = A \left(\frac{V_{\max}}{10 \text{ km s}^{-1}} \right)^{1.47}, \quad (3)$$

describes both populations well. For $V_{\max} > 15 \text{ km s}^{-1}$ and $R_{\max} > 0.5 \text{ kpc}$, the normalizations, A , differ by less than 3%.

¹ Throughout, we define M_v as the mass within a sphere of radius R_v that corresponds to an over density of 97 relative to the critical density.

Sample	A_{fit}	$A_{+68\%}$	$A_{-68\%}$
Isolated	0.747	1.09	0.521
Paired	0.704	1.00	0.499
Combined	0.725	1.06	0.511

Table 1. Fit results for the $R_{\text{max}} - V_{\text{max}}$ relationship defined in Equation 3. Listed are the normalizations resulting from fitting the data (Column 1) and from fitting the 68% scatter about that relation in bins of 100 points (Columns 2 and 3), separately for subhalos ($r < 300$ kpc) of the isolated and paired hosts, and when combining the datasets (the green lines in Figure 1).

Therefore, although the standard ELVIS runs lack the resolving power to determine inner differential density profiles, the integral properties of the halos of interest are well constrained. As pointed out by Di Cintio et al. (2013), however, the number of massive failures is dependent on the individual subhalo density profiles. We therefore investigate both the NFW profile and a range of Einasto profiles. We primarily present results with $\alpha = 0.18$, which Springel et al. (2008) showed is generally a slightly better fit to subhalos in ultra-high resolution DM-only simulations than an NFW profile, but also use $\alpha = 0.15$ as an example of a peaky Einasto profile and $\alpha = 0.28$ to sample flatter density profiles (this range also encompasses the results of Gao et al. (2008) and Navarro et al. (2010), though both works investigated more massive halos). We will see below that, while exact numbers may depend strongly on the assumed density profile, our overall conclusions hold for all profiles in this regime.

3 $R_{\text{max}} - V_{\text{max}}$ RELATIONSHIPS

As stated above, the parameters R_{max} and V_{max} , plus an assumed functional form for the density profile, fully define the circular velocity curve of a halo. The relationship between these parameters is therefore fundamental to the TBTF problem. In this section, we present fits to R_{max} as a function of V_{max} and compare the paired and isolated samples to search for biases in the structure of dwarf halos related to the environments of their hosts.

3.1 Subhalo scaling relations within 300 kpc

Though the ELVIS Suite contains 48 MW-size halos, only those in the paired sample are truly fair comparisons to the MW. However, GK14 showed that subhalo counts at fixed mass are identical between the two samples (when controlling for the host mass); we therefore begin by comparing the structural properties of subhalos of isolated and paired hosts to determine if the samples may be combined when counting massive failures within 300 kpc of the hosts.

Figure 1 plots the relationship between R_{max} and V_{max} for all subhalos within 300 kpc of the ELVIS hosts. Subhalos of the isolated hosts are plotted as magenta squares and those of hosts in LGs are indicated by black circles. The green line plots a fit to all the subhalos, holding the slope fixed to that in Equation 3; the dashed lines indicate the 68% scatter about that relation, calculated in running bins of 100 subhalos. The normalization of the fit, along with

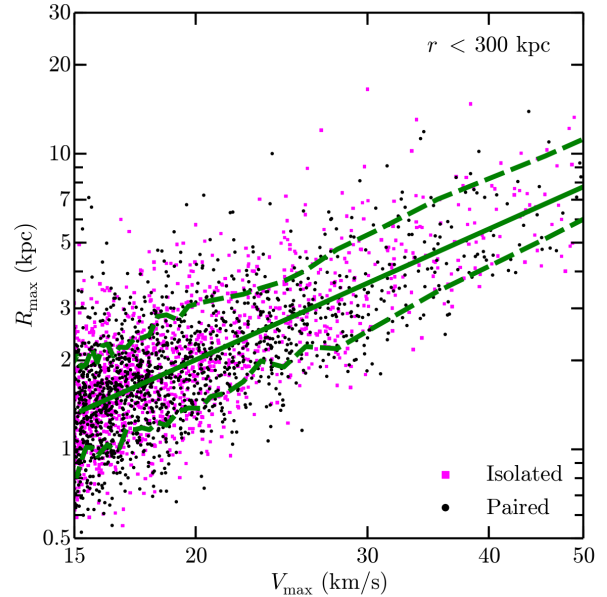


Figure 1. The relationship between R_{max} and V_{max} for subhalos in the ELVIS Suite within 300 kpc of each host. Subhalos near the paired hosts are plotted as black circles; those near isolated hosts are indicated by magenta squares. The thick green line plots the fit to all the halos and the dotted green lines encompass 68% of the points; the fits to these relations and the isolated and paired populations separately are given in Table 1. As the two datasets follow nearly identical relations and have consistent mass functions within the virial radii (GK14), we will combine the samples for better statistics when counting discrepant halos within 300 kpc of the hosts.

that of fits to the scatter above and below the relation, are given in Table 1 separately for the two populations, which differ only at the 5% level, and when combining the datasets. Any variance between subhalos of isolated and paired halos is well within the intrinsic scatter, and we therefore perform the remainder of our analysis within 300 kpc using subhalos of both isolated and paired hosts to maximize our statistics.

Because the subhalo properties in the paired and isolated system agree, we find no evidence that the results of Boylan-Kolchin et al. (2011, 2012) are affected by their study of isolated hosts. However, at the typical size of a TBTF halo ($V_{\text{max}} \sim 30 - 50 \text{ km s}^{-1}$), the median R_{max} of a subhalo in the ELVIS systems is 25% – 30% larger than those in the Aquarius simulations, consistent with the offset in σ_8 (Zentner & Bullock 2003; Polisensky & Ricotti 2014). This allows each dwarf to live in more massive hosts, and will lead to fewer discrepant halos. We will discuss this further in Section 4.1.

3.2 Halo scaling relations in the Local Field

GK14 showed that there are systematic differences between the environments surrounding isolated and paired halos, but did not compare the internal structure of halos in each environment. We therefore search for biases in the Local Field (LF) related to the larger-scale environments by compar-

Sample	A_{fit}	$A_{+68\%}$	$A_{-68\%}$
Isolated	1.016	1.443	0.723
Paired	0.994	1.437	0.709
Combined	1.005	1.448	0.719

Table 2. The normalizations for the $R_{\text{max}}-V_{\text{max}}$ relationship (Equation 3) in the Local Field as well as fits to the envelope that contains 68% of the halos, as in Table 1. For the paired systems, the Local Field is defined as the region within 1.2 Mpc of either host, but excluding all subhalos within 300 kpc of both hosts; the isolated “Local Fields” include all halos within 1.2 Mpc of the main host only, again excluding all subhalos within 300 kpc.

ing the relationship between R_{max} and V_{max} for field halos around isolated MWs and those in LGs.

Figure 2 plots this relationship in the LF (the region within 1.2 Mpc of either giant, but more than 300 kpc from both). The relation is again well fit by a power law with a log slope of 1.47 (Equation 3); such a fit is plotted as a light blue line and the 68% scatter about that fit, again calculated in running bins of 100 halos, is indicated by the dashed lines. As expected from tidal stripping arguments (see Zentner & Bullock 2003; Kazantzidis et al. 2004; Diemand et al. 2007), the average densities of field halos are significantly lower than subhalos at fixed V_{max} , as can be seen from the green line, which indicates the fit within 300 kpc plotted in Figure 1. We again fix the slope of the fits and find the normalizations given in Table 2.

Although the normalizations presented in Table 2 for the isolated and paired samples agree at the percent level, GK14 showed that the number counts do not agree beyond the virial radius of each host. As we are explicitly concerned with both the number and structure of field halos, we will use only those surrounding the paired hosts to count massive failures in the LF. Moreover, as in GK14, we will exclude the two systems with a third large halo in the Local Volume (Siegfried & Roy and Serena & Venus) when studying the LF. However, the apparent lack of structural differences indicates that detailed ultra-high resolution simulations of isolated dwarf galaxies in the field should be accurate analogs to Local Field dwarfs that have not yet interacted with either giant.

4 MASSIVE FAILURES IN THE ELVIS SUITE

4.1 Counting massive failures within 300 kpc

Qualitatively, we are concerned with counting halos that are massive enough that they should have formed stars, but that have no obvious luminous counterparts in the local Universe. We select halos with $V_{\text{peak}} > 30 \text{ km s}^{-1}$ as “massive enough” because halos larger than 30 km/s should be able to retain substantial gas in the presence of an ionizing background and therefore, *in principle*, should form stars (Babul & Rees 1992; Efstathiou 1992; Thoul & Weinberg 1996; Gnedin 2000; Okamoto et al. 2008); however, we must also carefully define the criteria to be a “luminous counterpart” of a galaxy in our sample. In what follows, we describe two ways of counting subhalos that have no obvious luminous counterparts.

As in Boylan-Kolchin et al. (2011), our observational

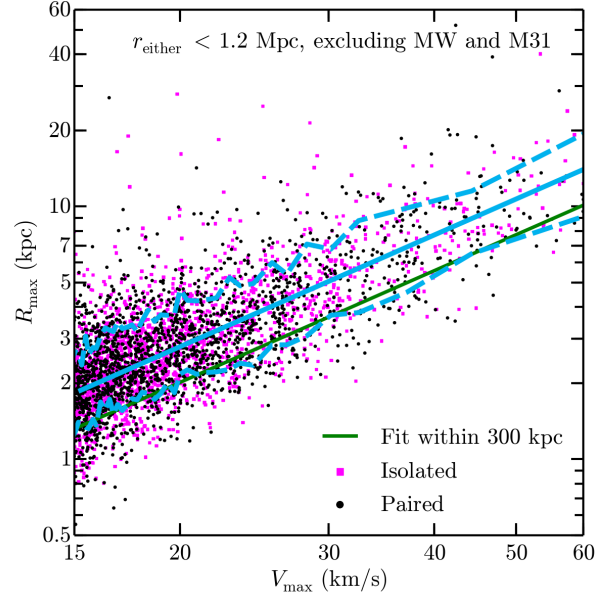


Figure 2. Identical to Figure 1, but plotting the relationship between R_{max} and V_{max} of halos that reside in the Local Field – the region within 1.2 Mpc of either host, but more than 300 kpc from both giants. The cyan line plots a power-law fit to all the halos with a log slope held equal to that in Equation 3; the normalization for all the data and for the individual datasets, along with fits to the scatter (dashed lines) are given in Table 2. The green line plots the fit within 300 kpc, where halos are systematically denser at fixed V_{max} due to tidal stripping.

sample is comprised of the satellites within 300 kpc of the MW with $M_{\star} > 2 \times 10^5 M_{\odot}$, excluding the Sagittarius dwarf and the Magellanic Clouds. Sagittarius is currently undergoing an interaction with the MW disk and is therefore likely not in equilibrium; the dwarf irregular Magellanic Clouds are removed from the sample because satellites as large as the Magellanic Clouds are rare around MW-size hosts (Boylan-Kolchin et al. 2010; Busha et al. 2011; Tollerud et al. 2011), and therefore do not have corresponding subhalos in many of the ELVIS systems. Our observational sample is thus likewise comprised of nine galaxies with $L > 10^5 L_{\odot}$: the classical dSphs and Canes Venatici (CVnI).

We now turn to the problem of assigning galaxies to subhalos, and identifying subhalos without luminous counterparts. The original formulation of TBTF counted unidentified subhalos as objects with circular velocity profiles that were at least 2σ above the observed circular velocity of each dwarf at its half-light radius ($V_{1/2} = V_{\text{circ}}(r = r_{1/2})$). These subhalos clearly lack observational counterparts. We will adopt a similar counting procedure, but instead use 1σ errors to define over-dense outliers. Specifically, we will refer to subhalos with $V_{\text{peak}} > 30 \text{ km s}^{-1}$ that are more than 1σ denser (at $r_{1/2}$) than any of the MW dwarfs as “strong massive failures”.

This “strong massive failure” formulation, which mirrors that originally used in Boylan-Kolchin et al. (2011, 2012), is particularly conservative. By counting only subhalos that are denser than all of the MW dwarfs, it ignores the potentially large number of subhalos that are consis-

tent with hosting only the densest observed dwarfs. Most MW-size hosts contain several subhalos that can *only* host either Draco or Ursa Minor, but nothing else. Since clearly only one halo can actually host Draco, this way of counting under-estimates the magnitude of the problem. Moreover, the “strong massive failure” definition is highly dependent on a single object, the densest MW dSph (Draco). If Draco did not exist, the strong massive failure count would be much larger. Similarly, if Draco were twice as dense, the strong massive failure count would approach zero. Ideally, we would like to find a measure that is less sensitive to the properties of a single object.

With these issues in mind, we introduce a second way of counting unidentified massive subhalos, which we refer to as the “massive failure” count. These are halos that were massive at infall (with $V_{\text{peak}} > 30 \text{ km s}^{-1}$) and that have no observational counterpart after each dense satellite is assigned to a single subhalo. Specifically, we find all halos that are *at least* as dense as Draco and Ursa Minor (in practice this demands that today halos have $V_{\text{max}} \gtrsim 25 \text{ km s}^{-1}$). We then examine the subset that are consistent with either Ursa Minor or Draco and remove the most massive possible counterpart to those galaxies. The remaining set allows us to enumerate unaccounted-for, yet massive, halos. We will discuss the impact of selecting Draco and Ursa Minor for this process below.

To summarize, we will count two classes of discrepant halos in the ELVIS Suite. **Strong massive failures** are too dense to host any of the bright MW dSphs, with circular velocities at $r_{1/2}$ that are above the 1σ constraints for all the dwarfs in the sample. **Massive failures** include all strong massive failures plus all massive halos that have densities consistent with the high density dwarfs (Draco and Ursa Minor) but that can’t be associated with them without allowing a single galaxy to be hosted by multiple halos. For typical profiles, subhalos with $V_{\text{max}} \lesssim 25 - 30 \text{ km s}^{-1}$ can host a low density dwarf, and thus are never selected as a massive failure; the **massive failures** are therefore generally subhalos that started out dense ($V_{\text{peak}} > 30 \text{ km s}^{-1}$) and remain dense ($V_{\text{max}} \gtrsim 25 \text{ km s}^{-1}$) at $z = 0$.

Figure 3 provides an illustration of these definitions. Shown are rotation curves of all $V_{\text{peak}} > 30 \text{ km s}^{-1}$ halos identified within 300 kpc of an $M_v = 1.3 \times 10^{12} M_\odot$ halo (Douglas, a paired host in the ELVIS sample). The solid black lines and solid cyan lines plot massive failures; the latter are *strong* massive failures because they are denser than every dwarf. The dotted curves indicate subhalos that had $V_{\text{peak}} > 30 \text{ km s}^{-1}$ but that are *not* massive failures – the magenta dotted lines are those selected to host Draco and Ursa Minor, and the grey dotted lines plot systems that have been stripped enough to host the lower density galaxies at $z = 0$. The curves correspond to Einasto profiles with $\alpha = 0.18$, normalized using the measured R_{max} and V_{max} values for each identified system. The dashed grey line indicates the lone Magellanic Cloud analog in Douglas, defined as subhalos with present day $V_{\text{max}} > 60 \text{ km s}^{-1}$ (Stanimirović et al. 2004), which is eliminated from our analysis. Our cut is again less conservative than that in Boylan-Kolchin et al. (2011): the criterion used by those authors would eliminate approximately one additional subhalo per host, on average (i.e. they would measure one fewer strong massive failure per host).

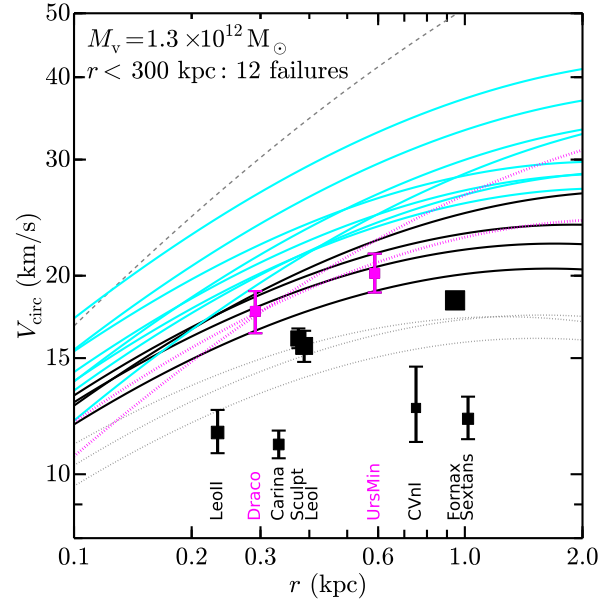


Figure 3. Rotation curves, assuming Einasto profiles with $\alpha = 0.18$, of all resolved halos with $V_{\text{peak}} > 30 \text{ km s}^{-1}$ within 300 kpc of the center of Douglas (based on measured V_{max} and R_{max} values in the simulation). Plotted as black points are the data for the MW satellites brighter than $2 \times 10^5 L_\odot$ compiled in Wolf et al. (2010), with sizes proportional to the log of their stellar masses. The cyan lines indicate strong massive failures – subhalos that are too dense to host *any* of the MW dSphs. The black lines plot the additional subhalos that are identified as massive failures according to the stricter definition given in the text: halos with $V_{\text{peak}} > 30 \text{ km s}^{-1}$ that are not accounted for by the dense galaxies in the observational sample. The subhalos with $V_{\text{peak}} > 30 \text{ km s}^{-1}$ that are selected to host the high density galaxies, Draco and Ursa Minor, are indicated by dotted magenta lines, with their associated galaxies plotted as magenta squares. The dotted lines plot the subhalos that are consistent with at least one of the remaining seven dwarfs in our sample, which are allowed to reside in multiple such subhalos. The grey dashed line indicates the sole subhalo of Douglas expected to host a Magellanic Cloud ($V_{\text{max}} > 60 \text{ km s}^{-1}$), which we exclude from our analysis. Not plotted are 40 resolved ($V_{\text{max}} > 15 \text{ km s}^{-1}$) subhalos with $V_{\text{peak}} < 30 \text{ km s}^{-1}$. In all, Douglas hosts twelve unaccounted-for massive failures, including eight strong massive failures that are too dense to host any bright MW dSph.

The data points in Figure 3 indicate measurements of $V_{1/2}$ at $r_{1/2}$ for the MW dSphs in our sample (taken from Wolf et al. 2010, who used data from Walker et al. 2009 along with data from Muñoz et al. 2005; Koch et al. 2007; Simon & Geha 2007 and Mateo et al. 2008).² The points are sized by the log of the stellar mass of each galaxy. Plotted in black are the low density MW dSph galaxies. The magenta

² For simplicity, we exclude galaxies within 300 kpc of M31 – many of the M31 satellites have substantial contributions from baryons within $r_{1/2}$, making a measurement of the central dark matter density very difficult. However, the central masses of the M31 dSphs appear to be consistent with the MW dSphs (Tollerud et al. 2012), and are therefore inconsistent with the subhalos expected to host them (Tollerud et al. 2014).

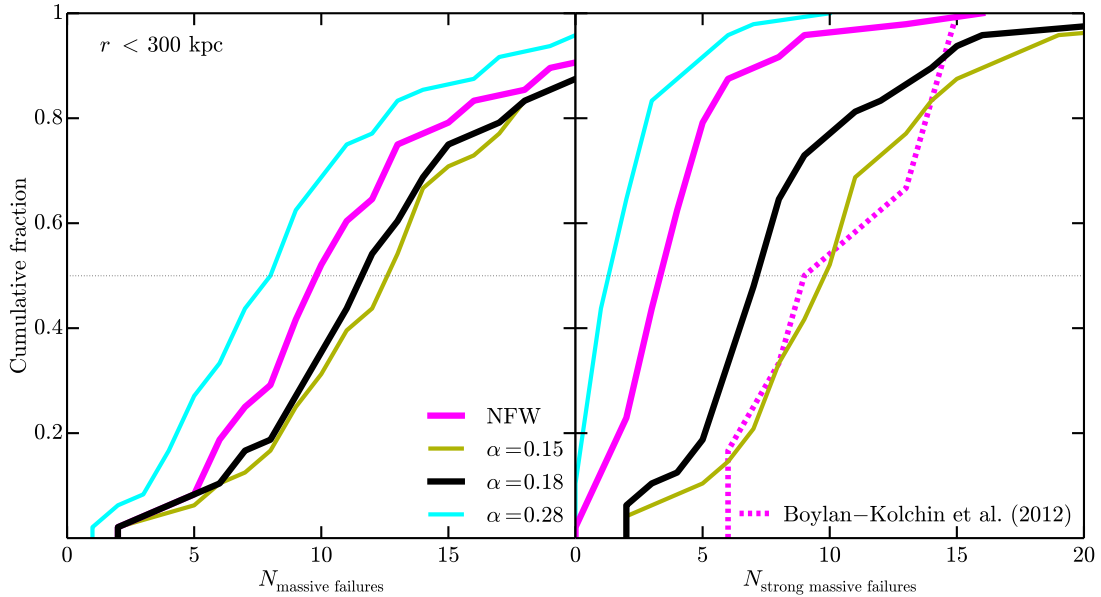


Figure 4. The fraction of hosts (out of 48) with fewer than N massive failures on the left and N strong massive failures on the right within 300 kpc of each host, as a function of N . Plotted are results assuming an NFW density profile (magenta) and Einasto profiles with $\alpha = 0.15$ (dark yellow), 0.18 (black), and 0.28 (cyan). In the left panel, we plot the number of strong massive failures in the Aquarius hosts as a dashed magenta line. Less than 10% of the ELVIS hosts contain no strong massive failures and we predict ~ 12 massive failures within 300 kpc of the MW.

points indicate the high density dSphs, Draco and Ursa Minor, which may only be associated with a single subhalo in each host (indicated by the dotted magenta lines) when counting massive failures. If the data points for Draco or Ursa Minor were 10 km s^{-1} higher, the strong massive failures (cyan lines) would vanish but the number of massive failures (cyan and black lines) would remain unchanged.

Figure 4 summarizes the results of counting massive failures in the complete set of forty-eight hosts, where each line corresponds to a different assumed density profile shape. Black lines show results for our fiducial choice, an $\alpha = 0.18$ Einasto profile; also shown are the implied distributions for NFW profiles (magenta), an underdense Einasto (cyan; $\alpha = 0.28$), and an overdense Einasto (dark yellow, $\alpha = 0.15$). The left panel indicates the cumulative distribution of massive failures and the right plots the same for strong massive failures; also plotted as a dashed magenta line is the distribution of 1σ discrepant subhalos from the Aquarius simulations, which we discuss below. As explained above, the strong definition is highly sensitive to the densest dwarf; it is likewise strongly dependent on the density profile, with medians varying between 2 and 10 for those chosen here. The number of massive failures, however, is more consistent and varies by a maximum of ~ 5 – the median varies from 8.5 for $\alpha = 0.28$ to 13 for $\alpha = 0.15$.

All of the forty-eight hosts contain at least two strong massive failures for $\alpha = 0.18$; using the slightly less dense NFW profile results in only one (iHera, with $M_v = 1.22 \times 10^{12} M_\odot$) of the forty-eight hosts (2%) containing no strong massive failures. Even the least dense profile considered here ($\alpha = 0.28$) leads to only five hosts (10%) with no strong

failures.³ These results are similar to the expectations of Purcell & Zentner (2012), who estimated the prevalence of strong massive failures in Milky-Way size hosts using a semi-analytic formalism, though in detail we have found slightly higher fractions of systems with strong massive failures.

The problem is revealed as more serious when we enumerate all unaccounted-for massive halos, however. None of the ELVIS hosts are without massive failures: the least problematic MW analogs host ~ 3 dense subhalos without bright counterparts – more than twice the number of known dense satellites. Unless the spatial distribution of dense satellites is highly anisotropic such that their on-the-sky density drastically increases behind the plane of the disk, it is unlikely that this disagreement can be reconciled via incompleteness arguments. However, one explanation of the observed lack of bright satellites between 100 – 400 kpc of the MW (Yniguez et al. 2013) is that there are as many as ~ 10 missing MW satellites with $L > 10^5 L_\odot$ – TBTF may be explained if the majority of these missing galaxies are as dense or denser than Draco, though there is no a priori reason to believe this to be the case.

The choice of Draco and Ursa Minor as our high-density dwarfs is based on the observation that they are the only two systems that demand to be hosted by $V_{\text{max}} > 20 \text{ km s}^{-1}$ halos to high significance. Nevertheless, it is useful to investigate how our massive failure count would change if we altered this choice. The number of massive failures shrinks if only Draco or only Ursa Minor is selected to be uniquely

³ For completeness sake, we note that the massive failures are drastically reduced in number or disappear completely if we assume a strongly cored or flat inner profile ($\alpha = 0.5 - 1$).

hosted (the medians vary between 5 – 11 for Draco only and 6 – 11 for Ursa Minor only), but adding more dSphs to this list identifies only a few more subhalos as massive failures: including the three additional galaxies with $V_{1/2} > 15 \text{ km s}^{-1}$ (Fornax, Leo I, and Sculptor) raises the median per host to only 11 – 13. That is, there are ~ 10 subhalos per host as dense or denser than Draco and Ursa Minor, but there are only $\lesssim 4$ additional subhalos with central densities similar to Fornax, Leo I, and Sculptor that have reached $V_{\text{peak}} \geq 30 \text{ km s}^{-1}$.

Our results are consistent with the expectation that lowering σ_8 helps to alleviate TBTF. The distribution of the number of strong massive failures in the Aquarius hosts is plotted as the dotted magenta line in Figure 4. As in Boylan-Kolchin et al. (2012), NFW profiles have been assumed in the inner region of the halos. Though the sample size is much smaller (6 instead of 48), there are significantly more massive failures in the WMAP-1 cosmology than result from the updated WMAP-7 values, in agreement with Lovell et al. (2013) and Polisensky & Ricotti (2014). Note, however, that the σ_8 we have adopted (based on WMAP-7) is somewhat lower than the favored value from the first-year Planck results (Planck Collaboration et al. 2013), and even so the number of massive failures remains high.

We have also checked for correlations with host mass, and find a weak positive correlation, as expected from the scaling of the subhalo mass function. The scatter about the trend is very large, but an extrapolation of the fit suggests that the MW mass must be below $\sim 7 \times 10^{11} M_{\odot}$ to eliminate the massive failures (see also Boylan-Kolchin et al. 2012; Wang et al. 2012; Purcell & Zentner 2012), which is in conflict with large-scale dynamical mass estimates of the MW (van der Marel et al. 2012; Boylan-Kolchin et al. 2013, and references therein).

4.2 Massive failures in the Local Field

4.2.1 Counting discrepant field halos

Now we extend our count of expected massive halos to the Local Field (LF) – a volume defined to be within 1.2 Mpc of either giant host, but excluding 300 kpc spherical regions around each in order to avoid satellites (and thus the potential for large tidal influences). Figure 5 is analogous to Figure 3, in that it compares halos within the LF of the ELVIS pair Zeus & Hera to observed galaxies within the same volume around the MW and M31. In GK14, we showed that the Zeus & Hera pair provides a good match to the observed stellar mass function in the Local Group when abundance matching is applied (see Figure 9 of GK14). The open light blue data points plot constraints on $V_{1/2}$ at $r_{1/2}$ for the ten dark matter-dominated galaxies in the LF with measured line-of-sight stellar velocity dispersions, σ_* , again with sizes proportional to the log of their stellar masses.⁴

There are four known galaxies that meet the distance cuts but that we exclude from our analysis: NGC 6822, Sagittarius dIrr, Andromeda XVI, and Phoenix. Of these four, all but NGC 6822 lack definitive mass measurements. The galaxy NGC 6822 is baryon dominated (Kirby et al.

2014) and we exclude it because determining its dark matter mass is difficult and because its host halo is likely to have undergone adiabatic contraction. There have been no attempts to measure the stellar velocity dispersion of the Sagittarius dIrr galaxy. Letarte et al. (2009) established an upper limit of $V_{1/2} < 17.3 \text{ km s}^{-1}$ at $r_{1/2} = 0.18 \text{ kpc}$ for Andromeda XVI, similar to the measurement for Leo T in (V_{circ}, r) space. In a conference proceeding, Zaggia et al. (2011) published $(V_{1/2}, r_{1/2}) \approx (14 \text{ km s}^{-1}, 0.6 \text{ kpc})$ for Phoenix, placing it between Aquarius and Cetus in Figure 5, and therefore among the lower density dwarfs. Therefore, our massive failure counts may be high by 3 (before accounting for incompleteness, which we discuss further in §4.2.2).

For the seven galaxies that are purely dispersion supported, we calculate $V_{1/2}$ from σ_* via the Wolf et al. (2010) formula. Velocity dispersions for the two Andromeda dwarfs with constraints on σ_* that meet the distance cuts are from Collins et al. (2013). Measurements for the field dwarfs are from Kirby et al. (2014) where available; the constraints on Leo T and Tucana are from Simon & Geha (2007) and Fraternali et al. (2009), respectively. Three of the field dwarfs – WLM, Pegasus, and Tucana – also display evidence of rotation support, and are therefore not well described by the Wolf et al. (2010) methodology. We use the result from Leaman et al. (2012) for WLM, who calculated the mass within $r_{1/2}$ with a detailed dynamical model. For the latter two, we follow Weiner et al. (2006) in replacing σ_*^2 with $\sigma_*^2 + \frac{1}{2}(v \sin i)^2$ when calculating $V_{1/2}$, where $v \sin i$ is the projected rotation velocity (see also §5.2 of Kirby et al. 2014).

The lines in Figure 5 plot the extrapolated rotation curves of the resolved dwarf halos with $V_{\text{peak}} > 30 \text{ km s}^{-1}$ around Zeus & Hera, again assuming an Einasto profile with $\alpha = 0.18$. That the lower-right section of the plot is empty is typical of the ELVIS fields – only ~ 10 -25% of the field halos that meet the “massive” cut ($V_{\text{peak}} > 30 \text{ km s}^{-1}$) have been sufficiently stripped to have $V_{\text{max}} < 25 \text{ km s}^{-1}$. Blue dotted lines indicate individual halos that are consistent with observed dwarfs; we do not count these systems as massive failures.

The black lines in Figure 5 indicates the massive failures in the Local Field. Due strictly to the published mass for Tucana, which is above *every* halo in the sample for $\alpha = 0.18$; there are no strong massive failures in the LFs around the ELVIS hosts.⁵ However, the systematic over-abundance of large halos remains: though Tucana eliminates any strong massive failures in the LF, the median number of halos per field that are consistent *only* with Tucana, i.e. the number of halos that would be identified as strong massive failures if Tucana did not exist, is 7.5, again assuming $\alpha = 0.18$. We will further show below that, if abundance matching holds at these masses, most of these galaxies should be bright ($M_* > 10^6 M_{\odot}$). Moreover, the lack of environmental stripping at larger radii leaves the vast majority of these objects with $V_{\text{max}} > 30 \text{ km s}^{-1}$ today.

The distribution of the number of massive failures in the Local Field is plotted in Figure 6. The number of halos that are naively expected to host luminous galaxies

⁴ See §4.2.2 for a summary of the origin of the M_* estimates.

⁵ The field around Scylla & Charybdis contains two halos with circular velocities that marginally exceed that of Tucana at $r_{1/2}$ if $\alpha = 0.15$, but they agree within 1σ .

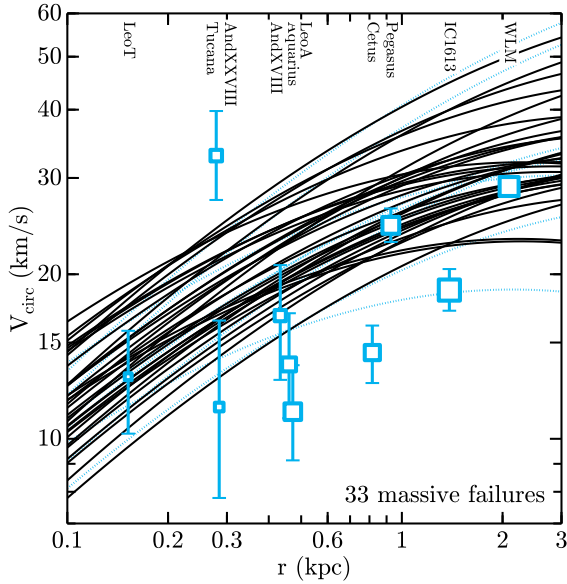


Figure 5. Rotation curves ($\alpha = 0.18$) for all resolved field halos in the LF around Zeus & Hera with $V_{\text{peak}} > 30 \text{ km s}^{-1}$ (extrapolated from measured V_{max} and R_{max} values in the simulation). Massive failures (unaccounted-for satellite halos that became large enough to form stars) are plotted as black lines; halos that are hosting one of the field dwarfs are indicated by light blue dotted lines. As in Figure 3, halos with $V_{\text{peak}} < 30 \text{ km s}^{-1}$ are not plotted – there are 254 such resolved halos in the Local Field around Zeus & Hera. The light blue points indicate the kinematic constraints on the galaxies in the LF; their sizes are again proportional to the log of the stellar mass of each galaxy. Many of the massive failures are denser than all the known field dwarfs except for Tucana.

($V_{\text{peak}} > 30 \text{ km s}^{-1}$) exceeds the number of known dwarfs by a factor $\gtrsim 2$ in every case – no system has fewer than thirteen massive failures, even for $\alpha = 0.28$. Importantly, the exact number is insensitive to the assumed profile, with the minimum count of massive failures varying only by ± 3 among the pairs studied here. In a relative sense, the LF massive failure counts are even more robust than the counts within 300 kpc. The minimum number of massive failures in the LF varies from 12 – 15 (depending on assumed profile shape) and the median number varies from 16 – 18.⁶

Of course, the count given in Figure 6 ignores massive failures within the virial radii of either M31 or the MW. In order to give a more complete picture of TBTF problem throughout the Local Group, Figure 7 plots the rotation curves of all the massive failures near Douglas (excluding only those within 300 kpc of its M31 analog, Lincoln); i.e. it combines Figure 3 with a plot equivalent to Figure 5. Plotted as black lines are massive failures within 300 kpc; the light blue lines plot massive failures in the LF. The black and light blue points again plot constraints on the MW satellites and

⁶ Unlike the situation within 300 kpc, the missing halos are not explained by cored profiles: due to the relatively large half-light radii of WLM and IC 1613, there are at least eleven massive failures in each LF, even assuming $\alpha = 1$.

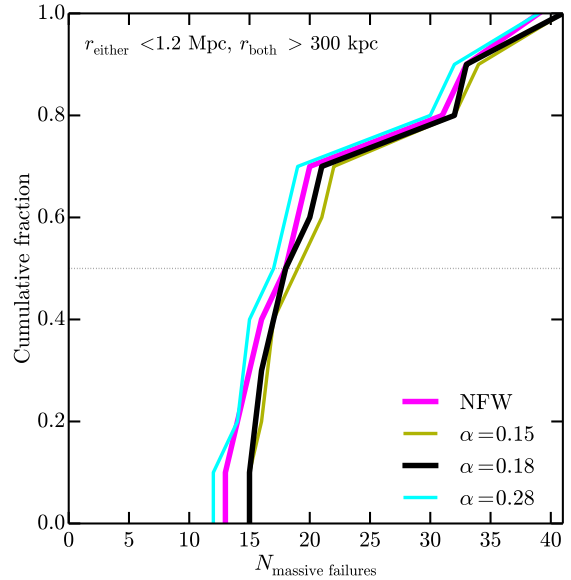


Figure 6. The distribution of the number of massive failures in the fields surrounding the ten LG analogs in the ELVIS pairs without a third giant nearby. Plotted are the number of field halos with $V_{\text{peak}} > 30 \text{ km s}^{-1}$ that do not have a corresponding bright galaxy in the field for the four profiles that we consider in this work; the colors are as in Figure 4. The ELVIS simulations predict that there are $\sim 18 - 20$ missing galaxies in the Local Field, many of which should be denser than the majority of the known field dwarfs (i.e. comparable to Tucana and Leo T).

galaxies in the LF, respectively. Halos selected to host those galaxies are not plotted. We have not included a comparison of the full Local Group including M31 satellites because, as explained above, M31 contains several baryon-dominated satellites, making the accounting more complicated. A more in-depth analysis of the M31 system is given in Tollerud et al. (2014).

Figure 8 provides an overview of the TBTF problem in the LG. As before, we combined the results of Figures 4 and 6, adding together the counts within 300 kpc and the Local Field for each MW analog, excluding the 300 kpc volume around the M31 analog. The distribution is therefore based on twenty virial volumes combined with ten LF analogs; none of these combinations contain fewer than thirteen massive failures. We find typically $\sim 26 - 34$ massive failures in the Local Volume, even excluding halos and galaxies within 300 kpc of M31. We find no trend between the number of massive failures within 300 kpc of a host and the number within the LF surrounding it.

Tides from disk interactions and ram pressure stripping are baryonic processes that have been invoked to lower the density of massive failure halos beyond what is predicted in dissipationless simulations (Zolotov et al. 2012; Arraki et al. 2013; Brooks & Zolotov 2012; Brooks et al. 2013). However, in the Local Field, particularly more than $\sim 500 \text{ kpc}$ from

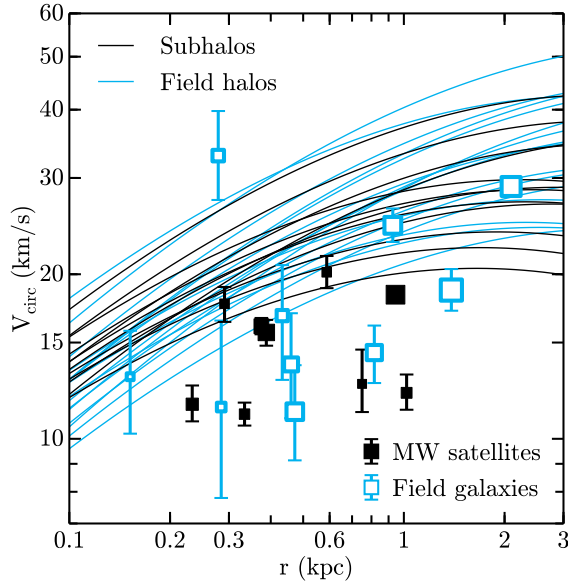


Figure 7. Plotted are the rotation curves for all halos identified as massive failures around Douglas, both within 300 kpc (black lines) and in the Local Field surrounding it (light blue lines), along with constraints on the dwarf galaxies in each region (black squares denote MW satellites and open light blue squares indicate field galaxies – sizes are again proportional to M_*); i.e. combining Figure 3 with a plot equivalent to Figure 5. Explicitly excluded are halos with $V_{\text{peak}} < 30 \text{ km s}^{-1}$; also not plotted are the halos selected to host a galaxy.

the nearest giant where the backplash fraction is below 50% (GK14), central halo densities should remain largely unaffected by tidal and ram pressure stripping. Moreover, Tucana, which shows evidence of having interacted with the MW (Teyssier et al. 2012), is the most dense galaxy in the field, calling into question proposed environmental mechanisms. Galaxies large enough to have affected their density profiles via supernovae feedback may be lurking unseen on the outer edge of the LF, but no galaxies brighter than $10^7 L_{\odot}$ have been discovered in the LF within the past fifty-five years (Pegasus dIrr; Holmberg 1958).

4.2.2 Missing galaxies in the Local Field?

In this Section, we present the stellar masses of those halos identified as massive failures, from abundance matching, and investigate whether they can be explained as unidentified dwarf galaxies in the LF. Though no galaxies have been discovered within the distance cut since the discovery of Andromeda XXVIII (Slater et al. 2011), the recent discovery of Leo P (Giovanelli et al. 2013; Rhode et al. 2013) at a distance of ~ 1.5 Mpc from the MW suggests that there may be new galaxies in the Local Volume that will be identified via HI observations or upcoming deep stellar surveys.

We begin by plotting the predicted stellar mass functions implied by our favored AM extrapolation from GK14, along with the observed stellar mass function of galaxies that meet the same radial cuts in the LG (in blue) in Fig-

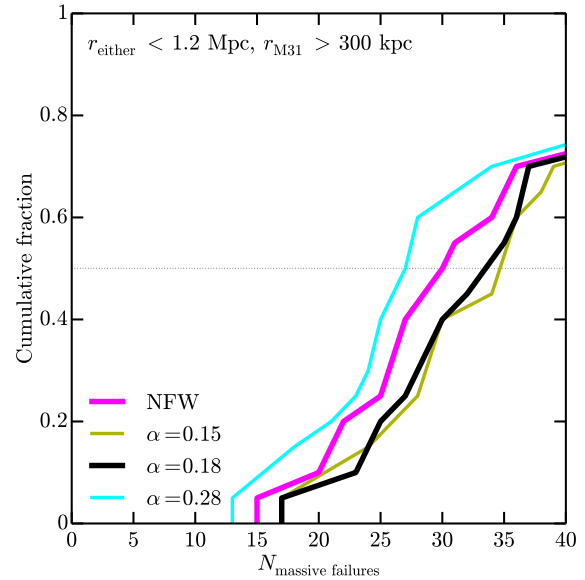


Figure 8. The distribution of the number of massive failures in each of twenty paired halos plus the field around them, i.e. combining results from Figures 4 and 6 but excluding failures that are within 300 kpc of the M31 analog. Colors are as in Figures 4 and 6. The exact number of massive failures depends on the specific density profile, but the conclusion that there are many missing large, dense halos in the Local Field is robust: each system has at least 14 massive failures, with a median between $\sim 26 - 34$.

ure 9.⁷ Stellar masses are from Woo et al. (2008) where available and are otherwise taken from the data cataloged in McConnachie (2012), assuming $M_*/L = 2$. We emphasize that the adopted AM relation does well in reproducing the observed stellar mass function above stellar masses $M_* = 4 \times 10^6 M_{\odot}$. The shaded region below this point draws attention to the region where the known census of galaxies lies below that predicted. Above this mass, however, the galaxy count around Zeus & Hera, the pair plotted in Figure 5 and highlighted in magenta in Figure 9, nearly matches that observed in the LF.

While a simple extrapolation of abundance matching creates a stellar mass function that agrees well with galaxy counts, *it does so by matching galaxies with halos that are too dense to reproduce the observed kinematics of those same galaxies* (see also Boylan-Kolchin et al. 2012). Specifically, it is difficult to match both the observed luminosity function and the observed densities of galaxies at the same time. The magnitude of the problem is demonstrated explicitly in Figure 10, which plots the stellar mass function of only the halos identified as massive failures (i.e. the stellar masses

⁷ We emphasize that the stellar mass range shown is large enough that an AM-inspired power-law relationship between M_* and M_v is well-motivated. Specifically, this is above the mass regime ($M_* < 10^6 M_{\odot}$, $V_{\text{peak}} < 30 \text{ km s}^{-1}$) where processes like reionization might act to “bend” the relation (Sawala et al. 2014; Garrison-Kimmel et al. 2014), possibly suppressing the count of faint galaxies in the Local Group.

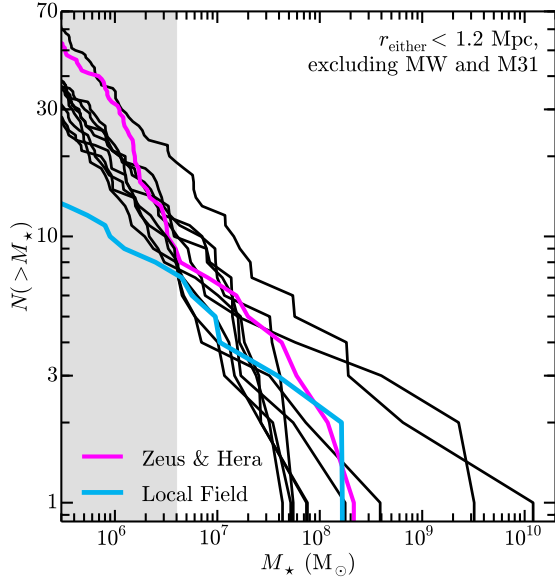


Figure 9. The stellar mass function observed in the Local Field (light blue) along with the stellar mass functions in the fields surrounding the ELVIS pairs, assuming the AM relation presented in GK14. The shaded region indicates stellar masses where the current census of galaxies lies below that of all the ELVIS pairs, $M_* < 4 \times 10^6 M_\odot$; at this mass, however, the count of known field galaxies nearly matches that around Zeus & Hera (highlighted in magenta), the LF shown in Figure 5.

associated with the black lines in Figure 5, specifically with $\alpha = 0.18$.) This is the subset of the stellar mass function⁸ shown in Figure 9 that includes only $V_{\text{peak}} > 30 \text{ km s}^{-1}$ halos that remain dense today ($V_{\text{max}} \gtrsim 25 \text{ km s}^{-1}$) and that are unaccounted for by any known galaxy. The takeaway point from Figure 10 is this: the TBTF halos should naively be hosting fairly bright galaxies, many of which should be more massive than $M_* \simeq 5 \times 10^6 M_\odot$.

As we show in the next section, based on the densities measured, the stellar mass of a galaxy does not seem to scale at all with the maximum circular velocity of the dark matter halo that it resides in. In the absence of baryonic processes that strongly affect halo densities, it is hard to understand how the relation could be as stochastic as it appears to be.

4.3 The $V_{\text{max}}-M_*$ relation in the Local Field

As the previous sections showed, it is likely that either there are roughly 15 dense galaxies living in high V_{max} halos in the Local Field that have yet to be discovered, or that the densities of $M_* \sim 10^{6.5} M_\odot$ field galaxies are much less dense than expected from straightforward Λ CDM predictions.

⁸ When selecting hosts for each galaxy, the candidate halos were sorted by M_* – that is, the halos plotted in Figure 10 are selected to have the *smallest* possible stellar masses. Nonetheless, the high mass end is largely unchanged from Figure 9, clearly showing that many of the massive failures are among the highest mass halos in the field and would naively be expected to host *bright* galaxies.

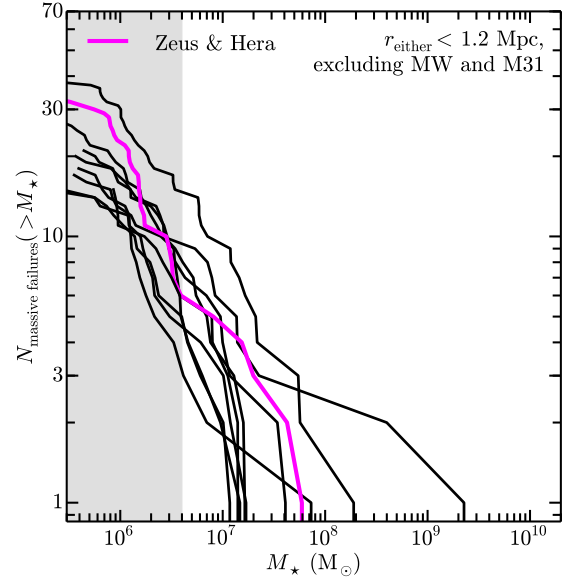


Figure 10. The stellar mass function, again from abundance matching, of the halos identified as massive failures in the LF; i.e. the black lines in Figure 5 counted in Figure 6. The magenta line again highlights the LF around Zeus & Hera. Even selecting those halos with the highest possible M_* to host the known dwarfs, the massive failures stellar mass functions are largely unchanged at the high mass end from Figure 9. Therefore, although the number count agree from $M_* \gtrsim 10^{6.5} M_\odot$, only lower mass field halos are kinematically compatible with the known LF galaxies.

In this subsection, we make this point explicitly by working out the inferred relationship between galaxy stellar mass and dark matter halo mass under the assumption that LF halos are unaffected by baryonic processes, and then compare that relationship to that expected from AM in the same volume.

Our approach is demonstrated in Figure 11, where the shaded bands show typical rotation curves for halos of various V_{max} values. The width of the bands correspond to the 1σ scatter R_{max} at fixed V_{max} given in Equation 3 and Table 2, assuming Einasto profiles with $\alpha = 0.18$. The points correspond to dwarfs and are identical to those in Figure 5 with sizes that are again proportional to their stellar masses. Note that the least luminous dwarf (Leo T) appears to reside in a fairly massive ($V_{\text{max}} \simeq 30 \text{ km s}^{-1}$) halo, while the galaxy IC1613, which is ~ 1000 times more luminous, appears to reside in a halo that is less massive ($V_{\text{max}} \simeq 20 \text{ km s}^{-1}$). Given the large errors in Leo T’s mass, the inferred halo sizes could be equal, but if there is any positive correlation between halo V_{max} and stellar mass, it must be extremely weak.

How does the implied relation compare to that expected from abundance matching? In Figure 12 we quantify the inferred relation, using the observational errors on dwarf masses together with the scatter in R_{max} at fixed V_{max} measured for LF halos in the ELVIS suite. Specifically, we plot the inferred V_{max} for each LF galaxy as a function of M_* as open light blue points. Error bars are 1σ . Due to its small half-light radius, Leo T may be hosted by any

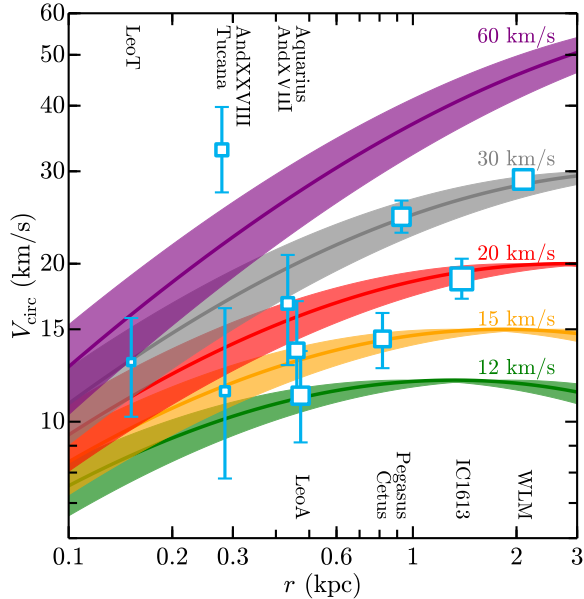


Figure 11. Typical rotation curves of halos in the Local Field for $\alpha = 0.18$, from the relations in Figure 2. Also plotted as open light blue points are the ten galaxies in the LF used in § 4.2.1 as in Figures 5 and 7; the points are again sized according to their stellar masses. The stellar masses of the halos do not appear to scale with V_{\max} , assuming a universal density profile.

halo with $V_{\max} \gtrsim 14 \text{ km s}^{-1}$ at the 1σ level, though the median relation predicts that it is hosted by a halo with $V_{\max} = 29 \text{ km s}^{-1}$. The upward arrows indicate the lower limits for Tucana and NGC 6822. Assuming the median relation between R_{\max} and V_{\max} , Tucana is incompatible with an Einasto profile with $\alpha = 0.18$ for all values of V_{\max} , though it may be hosted by a halo that is only a 1σ outlier. NGC 6822, as mentioned above, is dominated by baryonic mass within $r_{1/2}$ and is therefore unlikely to follow either an Einasto or NFW profile.

The circles in Figure 12 indicate theoretical expectations from the AM relation in GK14, the same relation that produces the *observationally-consistent* stellar mass function shown in Figure 9. The magenta circles highlight those halos around Zeus & Hera – the same halos that have a stellar mass function that masses the Local Group well in Figure 9.

Assuming that galaxies in the Local Field have density profiles of the kind predicted in our dissipationless simulations, any relation between V_{\max} and M_* for galaxies in the LF must be very weak (also see Strigari et al. 2008 and Boylan-Kolchin et al. 2012, who found similar results for MW satellites). This may suggest that the scaling between halo mass and stellar mass breaks down for small $M_* \lesssim 10^8 M_\odot$, but if the underlying relation followed something close to $M_* \sim V_{\max}^0$ over the mass range shown (and with a scatter similar to that shown in the data plotted) then this would drastically over-predicted the number of $M_* \sim 10^{6.5} M_\odot$ galaxies in the Local Group.

Another option is that the shape of the density profiles of the halos hosting LF galaxies vary strongly from system to system. Because these galaxies exist in the field, tidal

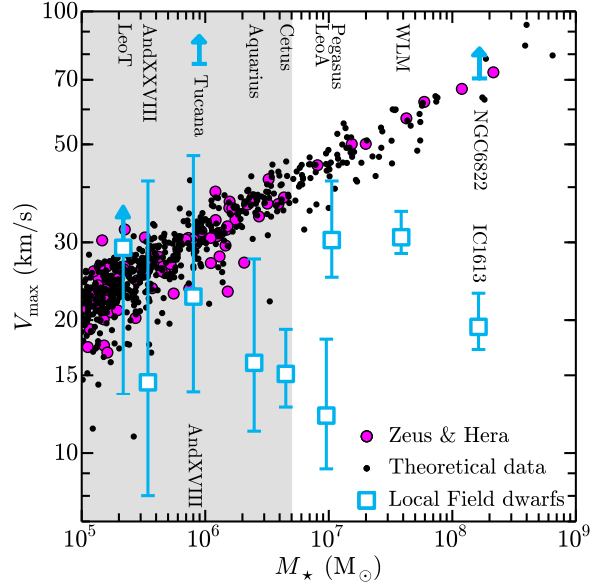


Figure 12. A comparison between the best-fit values of V_{\max} (assuming $\alpha = 0.18$) of the Local Field dwarfs to the stellar masses implied by the preferred AM relation in GK14. As expected, the latter follow a power law; the scatter is due to the scatter between V_{\max} and M_{peak} , upon which stellar masses are based. The former, however, appear to follow an extremely weak trend, indicating that stellar mass may not scale with V_{\max} at these low luminosities. Halos near Zeus & Hera are highlighted in magenta; the shaded region is the same as that in Figure 9. Due to the scaling of R_{\max} with V_{\max} , the measurement for Tucana is incompatible with the median relation; the 1σ bound is indicated by the arrow. Similarly, Leo T is unconstrained at the upper-end. The 1σ lower limit for NGC 6822 is also indicated, though it is baryon dominated and unlikely to be well described by an Einasto profile.

interactions and ram pressure stripping will not strongly affect their dark matter halos. Moreover, unless these galaxies formed with top-heavy initial mass functions or live in much smaller halos than abundance matching suggests, the energy available from supernovae is likely below that required to alter their density profiles significantly (Peñarrubia et al. 2012; Garrison-Kimmel et al. 2013).

We caution that the error bars in Figure 12 account only for the observational errors on $V_{1/2}$ and for the scatter in the $R_{\max} - V_{\max}$ relationship; that is, we are requiring that all galaxies reside in halos with identical density profile shapes. Additionally, we impose no sampling prior based on the predicted number of halos of a given V_{\max} , which would serve to shrink the error bars in Figure 12 and systematically push some of the inferred V_{\max} values lower (Martinez 2013). A more detailed analysis should be performed, but we leave that effort for future work.

5 CONCLUSIONS

In this paper, we have analyzed the structural properties of the small halos in the ELVIS Suite – both those within the virialized volumes of the two giant halos and those in the

fields surrounding them. Our results indicate that the Too Big to Fail problem, the discrepancy in central masses between the large subhalos of simulated MWs and the dSphs surrounding the MW, is an issue not only within 300 kpc, where environmental physics may be able to resolve the disagreement, but also in the Local Field, where such effects should be small. Specifically, we find that

- For NFW-like density profiles, nearly all of the ELVIS hosts contain at least one “strong massive failure” – satellite halos that are too dense to host any of the classical dSphs. The median number of strong massive failures per host is highly dependent on the assumed density profile, varying between 2 and 10, and would change dramatically if a dwarf much denser than Draco is discovered.

- The number of “massive failures,” $V_{\text{peak}} > 30 \text{ km s}^{-1}$ halos that remain dense at $z = 0$ and cannot be accounted for with the known census of dSphs, is much less dependent on the assumed profile. All of the ELVIS hosts contain at least one massive failure for the profiles considered in the work, with a median varying between 8.5 and 13. Unlike the count of strong massive failures, a newly discovered high-density dwarf would only alter these numbers by one.

- Though there are typically no strong massive failures in the Local Field (i.e. more than 300 kpc from both giants in the LG), the overall discrepancy between known galaxies that appear to live in dense (typically high mass) halos and the number of these halos predicted is even stronger. Most simulated LFs contain $\gtrsim 15$ more of these dense halos than can be accounted for observationally.

- If the discrepancy is to be resolved by discovering new galaxies, and *if* the stellar mass of a galaxy scales in a reasonable way with V_{max} , then the abundance matching technique predicts that there should be $\sim 2 - 10$ undiscovered galaxies with $M_{\star} > 10^7 M_{\odot}$ within the LF, though there have been none found since 1958. However, perhaps more puzzlingly, the stellar masses of the known field galaxies do not appear to correlate with the apparent V_{max} of their host halos, as estimated from $V_{1/2}$, suggesting either that the density profiles of the dwarfs vary strongly or that the scaling of M_{\star} with V_{max} breaks down at low luminosities.

The results presented in this work do not necessarily indicate the need to move beyond the standard Λ CDM model with collisionless dark matter. They can largely be viewed as predictions for results from future surveys, such as LSST and DES. However, if these missing dense galaxies are not discovered as we probe the nearby Universe to an increasing depth, these large dark matter halos must somehow be explained.

Acknowledgments

The authors thank Manoj Kaplinghat, Anna Nierenberg, Mike Cooper, Erik Tollerud, Arianna Di Cintio, Shunsaku Horiuchi, and Jose Oñorbe for helpful discussions.

Support for this work was provided by NASA through a *Hubble Space Telescope* theory grant (program AR-12836) from the Space Telescope Science Institute (STScI), which is operated by the Association of Universities for Research in Astronomy (AURA), Inc., under NASA contract NAS5-26555. This work was also supported by a matching equip-

ment grant from UC-HiPACC, a multicampus research program funded by the University of California Office of Research.

We also acknowledge the computational support of the NASA Advanced Supercomputing Division and the NASA Center for Climate Simulation, upon whose *Pleiades* and *Discover* systems the ELVIS simulations were run, and the *Greenplanet* cluster at UCI, upon which much of the secondary analysis was performed.

References

- Agnello A., Evans N. W., 2012, *ApJ*, 754, L39
 Amorisco N. C., Agnello A., Evans N. W., 2013a, *MNRAS*, 429, L89
 Amorisco N. C., Zavala J., de Boer T. J. L., 2013b, *arXiv:1309.5958* [astro-ph]
 Anderhalden D., Schneider A., Macciò A. V., Diemand J., Bertone G., 2013, *J. Cosmology Astropart. Phys.*, 3, 14
 Arraki K. S., Klypin A., More S., Trujillo-Gomez S., 2013, *MNRAS*
 Babul A., Rees M. J., 1992, *MNRAS*, 255, 346
 Behroozi P. S., Wechsler R. H., Conroy C., 2013c, *ApJ*, 770, 57
 Behroozi P. S., Wechsler R. H., Wu H.-Y., 2013a, *ApJ*, 762, 109
 Behroozi P. S., Wechsler R. H., Wu H.-Y., Busha M. T., Klypin A. A., Primack J. R., 2013b, *ApJ*, 763, 18
 Belokurov V. et al., 2007, *ApJ*, 654, 897
 Belokurov V. et al., 2006, *ApJ*, 647, L111
 Boylan-Kolchin M., Bullock J. S., Kaplinghat M., 2011, *MNRAS*, 415, L40
 Boylan-Kolchin M., Bullock J. S., Kaplinghat M., 2012, *MNRAS*, 422, 1203
 Boylan-Kolchin M., Bullock J. S., Sohn S. T., Besla G., van der Marel R. P., 2013, *ApJ*, 768, 140
 Boylan-Kolchin M., Springel V., White S. D. M., Jenkins A., 2010, *MNRAS*, 406, 896
 Boylan-Kolchin M., Springel V., White S. D. M., Jenkins A., Lemson G., 2009, *MNRAS*, 398, 1150
 Breddels M. A., Helmi A., 2013, *A&A*, 558, A35
 Brook C. B., Di Cintio A., Knebe A., Gottlöber S., Hoffman Y., Yepes G., Garrison-Kimmel S., 2013, *arXiv:1311.5492* [astro-ph]
 Brooks A. M., Kuhlen M., Zolotov A., Hooper D., 2013, *ApJ*, 765, 22
 Brooks A. M., Zolotov A., 2012, *arXiv:1207.2468* [astro-ph]
 Bullock J. S., 2010, *arXiv:1009.4505* [astro-ph]
 Bullock J. S., Kravtsov A. V., Weinberg D. H., 2000, *ApJ*, 539, 517
 Busha M. T., Alvarez M. A., Wechsler R. H., Abel T., Strigari L. E., 2010, *ApJ*, 710, 408
 Busha M. T., Wechsler R. H., Behroozi P. S., Gerke B. F., Klypin A. A., Primack J. R., 2011, *ApJ*, 743, 117
 Cen R., Gott, III J. R., Ostriker J. P., Turner E. L., 1994, *ApJ*, 423, 1
 Collins M. L. M. et al., 2013, *ApJ*, 768, 172
 Conroy C., Wechsler R. H., Kravtsov A. V., 2006, *ApJ*, 647, 201
 Davis M., Efstathiou G., Frenk C. S., White S. D. M., 1985, *ApJ*, 292, 371

- de Blok W. J. G., 2010, *Advances in Astronomy*, 2010
- Del Popolo A., 2012, *MNRAS*, 419, 971
- Del Popolo A., Lima J. A. S., Fabris J. C., Rodrigues D. C., 2014, arXiv:1404.3674 [astro-ph]
- Di Cintio A., Knebe A., Libeskind N. I., Brook C., Yepes G., Gottlöber S., Hoffman Y., 2013, *MNRAS*, 431, 1220
- Di Cintio A., Knebe A., Libeskind N. I., Yepes G., Gottlöber S., Hoffman Y., 2011, *MNRAS*, 417, L74
- Diemand J., Kuhlen M., Madau P., 2007, *ApJ*, 667, 859
- Efstathiou G., 1992, *MNRAS*, 256, 43P
- Einasto J., 1965, *Trudy Astrofizicheskogo Instituta Alma-Ata*, 5, 87
- Elbert O., Bullock J. S., Kaplinghat M., in prep, *MNRAS*
- Flores R. A., Primack J. R., 1994, *ApJ*, 427, L1
- Fraternali F., Tolstoy E., Irwin M. J., Cole A. A., 2009, *A&A*, 499, 121
- Frenk C. S., White S. D. M., Davis M., Efstathiou G., 1988, *ApJ*, 327, 507
- Gao L., Navarro J. F., Cole S., Frenk C. S., White S. D. M., Springel V., Jenkins A., Neto A. F., 2008, *MNRAS*, 387, 536
- Garrison-Kimmel S., Boylan-Kolchin M., Bullock J. S., Lee K., 2014, *MNRAS*, 438, 2578
- Garrison-Kimmel S., Rocha M., Boylan-Kolchin M., Bullock J. S., Lally J., 2013, *MNRAS*, 433, 3539
- Gelb J. M., Bertschinger E., 1994, *ApJ*, 436, 467
- Giovanelli R. et al., 2013, *AJ*, 146, 15
- Gnedin N. Y., 2000, *ApJ*, 542, 535
- Gottloeber S., Hoffman Y., Yepes G., 2010, arXiv:1005.2687 [astro-ph]
- Grcevich J., Putman M. E., 2009, *ApJ*, 696, 385
- Gritschneider M., Lin D. N. C., 2013, *ApJ*, 765, 38
- Gross M. A. K., Somerville R. S., Primack J. R., Holtzman J., Klypin A., 1998, *MNRAS*, 301, 81
- Hernquist L., Katz N., Weinberg D. H., Miralda-Escudé J., 1996, *ApJ*, 457, L51
- Holmberg E., 1958, *Meddelanden fran Lunds Astronomiska Observatorium Serie II*, 136, 1
- Jardel J. R., Gebhardt K., 2012, *ApJ*, 746, 89
- Jenkins A., Frenk C. S., White S. D. M., Colberg J. M., Cole S., Evrard A. E., Couchman H. M. P., Yoshida N., 2001, *MNRAS*, 321, 372
- Katz N., White S. D. M., 1993, *ApJ*, 412, 455
- Kauffmann G., White S. D. M., Guiderdoni B., 1993, *MNRAS*, 264, 201
- Kazantzidis S., Mayer L., Mastrogiuseppe C., Diemand J., Stadel J., Moore B., 2004, *ApJ*, 608, 663
- Kirby E. N., Bullock J. S., Boylan-Kolchin M., Kaplinghat M., Cohen J. G., 2014, arXiv:1401.1208 [astro-ph]
- Klypin A., Kravtsov A. V., Valenzuela O., Prada F., 1999, *ApJ*, 522, 82
- Klypin A. A., Trujillo-Gomez S., Primack J., 2011, *ApJ*, 740, 102
- Knollmann S. R., Knebe A., 2009, *ApJS*, 182, 608
- Koch A., Kleyna J. T., Wilkinson M. I., Grebel E. K., Gilmore G. F., Evans N. W., Wyse R. F. G., Harbeck D. R., 2007, *AJ*, 134, 566
- Koposov S. E., Yoo J., Rix H.-W., Weinberg D. H., Macciò A. V., Escudé J. M., 2009, *ApJ*, 696, 2179
- Kravtsov A., 2010, *Advances in Astronomy*, 2010
- Kravtsov A. V., Berlind A. A., Wechsler R. H., Klypin A. A., Gottlöber S., Allgood B., Primack J. R., 2004, *ApJ*, 609, 35
- Kuzio de Naray R., Kaufmann T., 2011, *MNRAS*, 414, 3617
- Kuzio de Naray R., McGaugh S. S., de Blok W. J. G., 2008, *ApJ*, 676, 920
- Larson D. et al., 2011, *ApJS*, 192, 16
- Leaman R. et al., 2012, *ApJ*, 750, 33
- Letarte B. et al., 2009, *MNRAS*, 400, 1472
- Lovell M. R., Frenk C. S., Eke V. R., Jenkins A., Gao L., Theuns T., 2013, arXiv:1308.1399 [astro-ph]
- Lunnan R., Vogelsberger M., Frebel A., Hernquist L., Lidz A., Boylan-Kolchin M., 2012, *ApJ*, 746, 109
- Martinez G. D., 2013, arXiv:1309.2641 [astro-ph]
- Mateo M., Olszewski E. W., Walker M. G., 2008, *ApJ*, 675, 201
- McConnachie A. W., 2012, *AJ*, 144, 4
- Moore B., 1994, *Nature*, 370, 629
- Moore B., Ghigna S., Governato F., Lake G., Quinn T., Stadel J., Tozzi P., 1999, *ApJ*, 524, L19
- Moster B. P., Naab T., White S. D. M., 2013, *MNRAS*, 428, 3121
- Muñoz R. R. et al., 2005, *ApJ*, 631, L137
- Navarro J. F., Frenk C. S., White S. D. M., 1996, *ApJ*, 462, 563
- Navarro J. F. et al., 2010, *MNRAS*, 402, 21
- Oñorbe J., Garrison-Kimmel S., Maller A. H., Bullock J. S., Rocha M., Hahn O., 2014, *MNRAS*, 437, 1894
- Okamoto T., Gao L., Theuns T., 2008, *MNRAS*, 390, 920
- Peñarrubia J., Pontzen A., Walker M. G., Koposov S. E., 2012, *ApJ*, 759, L42
- Planck Collaboration et al., 2013, arXiv:1303.5076 [astro-ph]
- Polisenky E., Ricotti M., 2014, *MNRAS*, 437, 2922
- Pontzen A., Governato F., 2012, *MNRAS*, 421, 3464
- Purcell C. W., Zentner A. R., 2012, *J. Cosmology Astropart. Phys.*, 12, 7
- Rhode K. L. et al., 2013, *AJ*, 145, 149
- Rocha M., Peter A. H. G., Bullock J. S., Kaplinghat M., Garrison-Kimmel S., Oñorbe J., Moustakas L. A., 2013, *MNRAS*, 430, 81
- Rodríguez-Puebla A., Avila-Reese V., Drory N., 2013, *ApJ*, 773, 172
- Sawala T. et al., 2014, arXiv:1404.3724 [astro-ph]
- Simon J. D., Geha M., 2007, *ApJ*, 670, 313
- Slater C. T., Bell E. F., Martin N. F., 2011, *ApJ*, 742, L14
- Somerville R. S., 2002, *ApJ*, 572, L23
- Springel V. et al., 2008, *MNRAS*, 391, 1685
- Springel V. et al., 2005, *Nature*, 435, 629
- Stanimirović S., Staveley-Smith L., Jones P. A., 2004, *ApJ*, 604, 176
- Strigari L. E., Bullock J. S., Kaplinghat M., Simon J. D., Geha M., Willman B., Walker M. G., 2008, *Nature*, 454, 1096
- Teyssier M., Johnston K. V., Kuhlen M., 2012, *MNRAS*, 426, 1808
- Thoul A. A., Weinberg D. H., 1996, *ApJ*, 465, 608
- Tollerud E. J. et al., 2012, *ApJ*, 752, 45
- Tollerud E. J., Boylan-Kolchin M., Barton E. J., Bullock J. S., Trinh C. Q., 2011, *ApJ*, 738, 102
- Tollerud E. J., Boylan-Kolchin M., Bullock J. S., 2014, arXiv:1403.6469 [astro-ph]
- Trachternach C., de Blok W. J. G., Walter F., Brinks E., Kennicutt, Jr. R. C., 2008, *AJ*, 136, 2720

- Vale A., Ostriker J. P., 2004, MNRAS, 353, 189
- van der Marel R. P., Fardal M., Besla G., Beaton R. L., Sohn S. T., Anderson J., Brown T., Guhathakurta P., 2012, ApJ, 753, 8
- Vera-Ciro C. A., Helmi A., Starkenburg E., Breddels M. A., 2013, MNRAS, 428, 1696
- Vogelsberger M., Zavala J., Loeb A., 2012, MNRAS, 423, 3740
- Walker M. G., Mateo M., Olszewski E. W., 2009, AJ, 137, 3100
- Walker M. G., Peñarrubia J., 2011, ApJ, 742, 20
- Wambsganss J., Bode P., Ostriker J. P., 2004, ApJ, 606, L93
- Wang J., Frenk C. S., Navarro J. F., Gao L., Sawala T., 2012, MNRAS, 424, 2715
- Warren M. S., Quinn P. J., Salmon J. K., Zurek W. H., 1992, ApJ, 399, 405
- Weiner B. J. et al., 2006, ApJ, 653, 1027
- Willman B. et al., 2005, AJ, 129, 2692
- Wolf J., Martinez G. D., Bullock J. S., Kaplinghat M., Geha M., Muñoz R. R., Simon J. D., Avedo F. F., 2010, MNRAS, 406, 1220
- Woo J., Courteau S., Dekel A., 2008, MNRAS, 390, 1453
- Yniguez B., Garrison-Kimmel S., Boylan-Kolchin M., Bullock J. S., 2013, arXiv:1305.0560 [astro-ph]
- Zaggia S., Held E. V., Sommariva V., Momany Y., Saviane L., Rizzi L., 2011, in EAS Publications Series, Vol. 48, EAS Publications Series, Koleva M., Prugniel P., Vauglin I., eds., pp. 215–216
- Zavala J., Vogelsberger M., Walker M. G., 2013, MNRAS, 431, L20
- Zentner A. R., Bullock J. S., 2003, ApJ, 598, 49
- Zolotov A. et al., 2012, ApJ, 761, 71

APPENDIX A: NUMERICAL CONVERGENCE

Three of the isolated hosts in the ELVIS Suite were re-simulated with eight times better mass resolution than the fiducial runs ($m_p = 2.35 \times 10^4 M_\odot$) and with a $z = 0$ softening length of 70 pc for the high resolution particles. Although the individual halo properties vary slightly between these HiRes simulations and the fiducial analogs, as expected from Oñorbe et al. (2014), we use those simulations here to determine the limits of our full sample. In Figure 13, we plot the relationship between R_{\max} and V_{\max} for subhalos within 310 kpc of these three hosts. We use 310 kpc to include a large subhalo that, owing to phase differences between the resolutions, is beyond 300 kpc at the standard resolution. Subhalos from the HiRes simulations are shown as cyan points and those from the standard resolution runs are plotted in black; the symbol types indicate the three host halos.

Fits to both of these populations, including only halos with $V_{\max} > 15 \text{ km s}^{-1}$ and $R_{\max} > 0.5 \text{ kpc}$, are also plotted in Figure 13. The power law given by Equation 3 fits both populations well, with a difference in the normalizations of less than 3%, indicating that our results are robust to resolution errors. We have also checked that our results do not depend on the specific halo finder by repeating this analysis with halo catalogs produced by *Amiga Halo Finder*

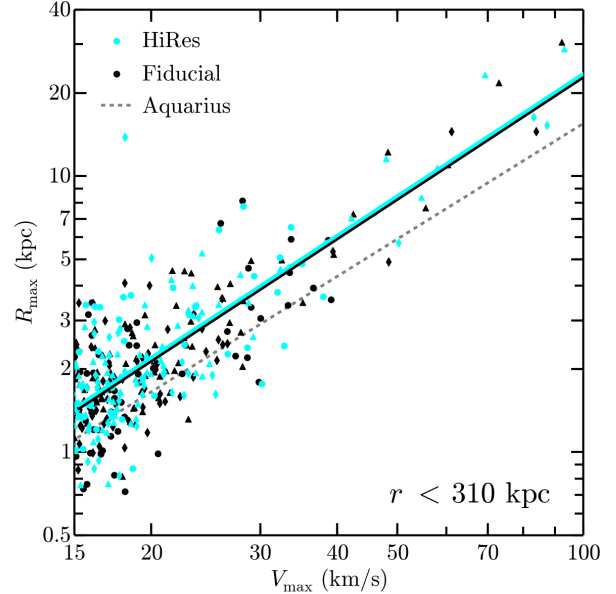


Figure 13. Resolution test comparing subhalos within 310 kpc of three of the isolated analogs in the ELVIS Suite, iKauket (circles), iHall (triangles), and iScylla (diamonds), at the standard resolution of the ELVIS suite (black points) and with eight times better mass resolution (cyan points); the fits to the data, weighted by V_{\max} , are also plotted. The normalizations of the fits to halos with $V_{\max} > 15 \text{ km s}^{-1}$ and $R_{\max} > 0.5 \text{ kpc}$ agree to within 3%, indicating that our results are not affected by numerical errors. The dashed grey line plots the relation found in Springel et al. (2008); the offset ($\sim 20\%$) is consistent with the updated σ_8 used in the ELVIS cosmology. We also find nearly identical relations using halo catalogs produced by AHF.

(Knollmann & Knebe 2009), which locates spherical overdensities in the three-dimensional matter distribution – the normalizations differ by 5% at most. *Rockstar* also appears to misidentify R_{\max} for a single small halo in the high resolution run; this halo, however, is not used in the full analysis and does not strongly bias the fit.

APPENDIX B: DENSITY PROFILES

Rather than individually fit profiles to each subhalo (an inaccurate approach, due to the insufficient resolution at low radii and relatively small differences in the profiles near R_{\max}), we perform our analysis using three Einasto profiles ($\alpha = 0.15, 0.18, \text{ and } 0.28$). As shown in Springel et al. (2008), an Einasto profile with α fixed at 0.18 is a better fit to most subhalos than a standard NFW profile – we therefore focus our efforts on this profile. Though a comprehensive analysis of the distribution of best-fit shape parameters of ultra-high resolution subhalos and field dwarfs does not exist in the literature, $\alpha = 0.15$ and 0.28 are the extreme values plotted in Springel et al. (2008) and we therefore consider those shape parameters as an estimate of appropriate scatter.

For a given α , the circular velocity may be expressed as a function of R_{\max} and V_{\max} , parameters which are ro-

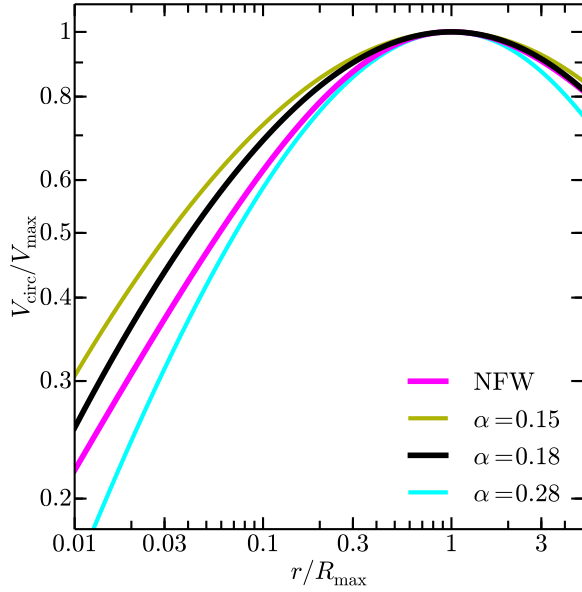


Figure 14. Circular velocities profiles, normalized by R_{\max} and V_{\max} for the three shape parameters considered above: $\alpha = 0.15$ (dark yellow), $\alpha = 0.18$ (black), and $\alpha = 0.28$ (cyan), along with that of an NFW profile (magenta). Smaller shape parameters result in denser halos, and therefore more massive failures.

bustly determined for the halos considered in this work (see Figure 13). For the Einasto profile,

$$\frac{V_{\text{circ}}^2(r)}{V_{\text{max}}^2} = \frac{4\pi/\alpha}{A(\alpha)B(\alpha)} \exp\left(\frac{2 - \log(8) + 3 \log(\alpha)}{\alpha}\right) \times \gamma\left(\frac{3}{\alpha}, \frac{2}{\alpha} \left(\frac{A(\alpha)r}{R_{\max}}\right)^\alpha\right) \frac{R_{\max}}{r}, \quad (4)$$

where $\gamma(x, y)$ is the lower incomplete gamma function. $A(\alpha)$ and $B(\alpha)$ relate V_{\max} and R_{\max} to r_{-2} and ρ_{-2} , the radius at which the log slope of the density profile is -2 and the density at that radius, via

$$\begin{aligned} R_{\max} &= A(\alpha)r_{-2} \\ V_{\max}^2 &= B(\alpha)G\rho_{-2}r_{-2}^2, \end{aligned} \quad (5)$$

By finding the maximum of Equation 4, one can show that $A(\alpha)$ is given by the root of

$$e^{-2x^\alpha/\alpha} \alpha^{\frac{\alpha-3}{\alpha}} x^3 - 8^{-1/\alpha} \gamma\left(\frac{3}{\alpha}, \frac{2x^\alpha}{\alpha}\right) = 0, \quad (6)$$

where $x = r/r_{-2}$. $B(\alpha)$ may then be obtained by directly calculating $V_{\text{circ}}(r)$ at R_{\max} . For $0 < \alpha < 1$, $A(\alpha)$ and $B(\alpha)$ are well fit by two-power functions:

$$\begin{aligned} A(\alpha) &= 1.715\alpha^{-0.00183}(\alpha + 0.0817)^{-0.179488} \\ B(\alpha) &= 9.529\alpha^{-0.00635}(\alpha + 0.3036)^{-0.206886} \end{aligned} \quad (7)$$

In Figure 14, we compare the resultant circular velocity curves for these three shape parameters, along with that of an NFW profile. Smaller values of α result in more mass near the center of halos and therefore lead to more unaccounted-for objects and massive failures in the simulations.